Macromolecules

pubs.acs.org/Macromolecules

Article

Planar Orientation and Transparency of Nanoporous-Crystalline Polymer Films

Baku Nagendra, Paola Rizzo, Christophe Daniel, and Gaetano Guerra*

Cite This: *Macromolecules* 2021, 54, 6605–6611

Read Online

ACCESS | Metrics & More | Article Recommendations | Supporting Information

ABSTRACT: The dependence of polymer film transparency on different kinds of planar orientations of nanoporous-crystalline (NC) phases of syndiotactic polystyrene (sPS) and poly(2,6-dimethyl-1,4-phenylene)oxide (PPO) is described. The two polymers exhibit opposite behavior: film transparency is improved for sPS and PPO by orientations of the chain axes of the NC phases being parallel ($c_{\parallel}$) and perpendicular ($c_{\perp}$) to the film plane, respectively. This behavior can be rationalized by the negative and positive birefringence of sPS and PPO chains, respectively. In fact, to maximize transparency, the refractive index of the NC phase along the perpendicular to the film plane has to be increased to come closer to that of the corresponding amorphous phase. This can be pursued by controlling the orientation of the NC phases and hence of the associated refractive index ellipsoids.

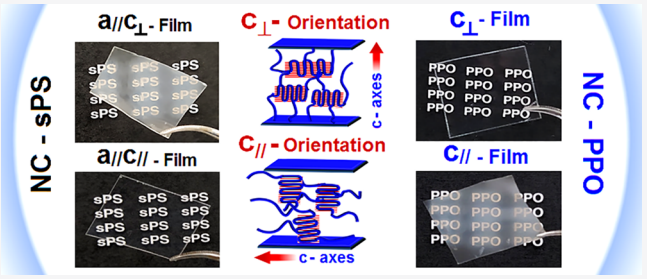

INTRODUCTION

Amorphous polymer films are generally highly transparent, due to their homogeneous refractive index. Semicrystalline polymer films, instead, exhibit a reduced transparency due to the different refractive index of their amorphous and crystalline phases. Inhomogeneous refractive indexes generate light scattering, thus reducing the amount of transmitted light.[1−5]

For most polymers, the density and hence refractive index of their crystalline phases are higher than for the corresponding amorphous phases ($n_{cr} > n_{am}$). In a few specific cases, e.g., isotactic poly(4-methyl-pentene-1),[6] the density and refractive index of crystalline and amorphous phases are similar, and hence, the film transparency is poorly affected by the degree of crystallinity. Only two polymers, syndiotactic polystyrene (sPS)[7−9] and poly(2,6-dimethyl-1,4-phenylene)oxide (PPO),[10,11] exhibit nanoporous-crystalline (NC) phases, with an ordered distribution of empty space, the density and hence refractive index of which are definitely lower than for the corresponding amorphous phases ($n_{NC} < n_{am}$).

Suitable procedures to increase the transparency of semicrystalline films generally imply a reduction of the crystal size to values smaller than the visible light wavelength, usually by adding nucleating agents.[1−5] The transparency of semicrystalline polymer films can be also improved by procedures (generally quenching) leading to mesomorphic polymer phases, like for isotactic polypropylene.[12,13] Another well-established method to obtain highly transparent films involves polymer crystallization under mechanical strain, being generally biaxial.[14−18] In fact, strain-induced crystallization in polymer films leads to formation of crystallites of nanometric size[19−23] as well as to a high degree of orientation (mainly of their crystalline phases), thus generating high optical anisotropy.[24−26]

Biaxial strain, as well as suitable solution crystallization processes, can lead to different kinds of *planar* or *uniplanar* orientations of the crystalline phases, exhibiting preferential orientation with respect to the film plane of a crystalline axis or of a crystalline plane, respectively.[27]

Planar and uniplanar orientations can be obtained, also without any mechanical stretching, for NC films of sPS[28−32] and PPO.[33,34] These crystalline phase orientations are obtained by cocrystallization procedures between the polymer host and low molecular mass guest molecules and are generally maintained after procedures of guest removal that lead to NC films.

The aim of this paper is to study the dependence of film transparency on the kinds of planar orientation of NC phases of sPS and PPO.

EXPERIMENTAL SECTION

sPS pellet (Trademark Xarec 90 ZC) was supplied by Idemitsu and has a weight-averaged molecular weight M_w = 197 kg/mol. PPO powder (P6130 grade) was supplied by Sabic and has an ultrahigh molecular weight M_w = 350 kg/mol.

Guest molecules dibenzyl ether (BE), benzene, carvone, limonene, chloroform ($CHCl_3$), 1,1,1-trichloroethane (TCA), 1,1,2-trichloroethylene (TCE), 1,2,4-trichlorobenzene (TCB), 1,2-dimethylbenzene (*o*-xylene), 1,4-dimethylbenzene (*p*-xylene), 1,2-dichloroethane

Received: April 27, 2021
Revised: June 9, 2021
Published: June 24, 2021

https://doi.org/10.1021/acs.macromol.1c00925
Macromolecules 2021, 54, 6605–6611

(DCE), and tetrahydrofuran (THF) were purchased from Aldrich and used without further treatment.

sPS cocrystalline (CC) films, with thicknesses in the range of 20−100 μm, were prepared by solution casting at room temperature from 0.2 to 0.8 wt % polymer solutions. Amorphous films with similar thickness were prepared by compression molding followed by quenching into ice water.

As for PPO, cocrystalline films with thicknesses in the range of 20−100 μm were obtained by two different procedures: (i) casting from solutions with 0.5−1 wt % polymer content and (ii) crystallization of amorphous PPO films, as induced by immersion in pure liquid guests. Amorphous PPO films were obtained by casting from 0.2 to 0.8 wt % chloroform solution at 60 °C.

sPS and PPO NC films were obtained from cocrystalline films by a typical guest extraction procedure: room temperature sorption−desorption of acetonitrile. The guest contents for CC films that were extracted to prepare NC films were in the range of ∼10−15 and ∼15−20 wt % for sPS and PPO, respectively. Complete guest removal was verified by the absence of guest peaks in the FTIR spectra of the extracted films.

Densities of polymer films were measured, after guest removal, by the flotation method. In particular, aqueous solutions of calcium dichloride and methanol were used to evaluate film densities higher and lower than 1 g/cm^3, respectively. Measured densities of the amorphous sPS and PPO films are 1.052 and 1.043 g/cm^3, respectively. Densities of the NC δ-form films of sPS are close to 0.99 g/cm^3. Densities of the NC α- and β-form films of PPO are close to 0.988 and 1.004 g/cm^3, respectively

WAXD data were obtained by a D8 QUEST Bruker diffractometer (CuKα radiation) and are shown as two-dimensional (2D) patterns. The reported 2D-WAXD patterns were collected by sending the X-ray beam parallel to the film surface (EDGE patterns).

The degree of planar orientation (f_c) of the prepared films was formalized by the Hermans orientation function

$$f_c = (\overline{3\cos^2\gamma} - 1)/2 \quad (1)$$

where $\cos^2\gamma$ was experimentally evaluated from EDGE patterns, by the azimuthal distribution of 010 and 001 reflections for sPS and PPO, respectively. In this framework, $f_c = 0$ corresponds to a random crystallite orientation, while $f_c = 1$ and $f_c = -0.5$ correspond to the c axes of all crystallites being parallel and perpendicular to the film plane, respectively.

Correlation lengths of crystalline domains D were evaluated for reflections with Miller indexes hkl, by the formula of Scherrer

$$D = (K\lambda)/(\beta_{hkl}\cos\theta_{hkl}) \quad (2)$$

where K is assumed equal to 0.9, λ = 0.154 18 nm (i.e., the wavelength of the used X-ray radiation), and β_{hkl} and θ_{hkl} are the full width at half-maximum (fwhm) and the diffraction angle of the considered hkl reflection Figure S1. X-ray patterns used for these D evaluations (Figure S1) and Table S1 collecting measured D values are shown in the Supporting Information (SI).

FTIR spectra were collected with a Vertex70 spectrometer from Bruker. The resolution was 2.0 cm^{-1} and 32 scans were averaged to reduce noise.

Differential scanning calorimetry (DSC) measurements were conducted with TA Q2000 equipment from TA Instruments, under controlled nitrogen gas flow, at a heating rate of 10 °C/min.

For evaluation of the degree of crystallinity of sPS and PPO films, methods based on two different techniques were used. In fact, for sPS we preferred evaluations based on FTIR spectra (Figure S2a,b, SI), as described in detail in ref 35. FTIR methods are much less accurate for PPO, due to more difficult spectral subtraction procedures. For PPO, we have used an evaluation method based on melting enthalpies, as obtained by DSC scans at a heating rate of 10 °C/min (Figure S2c,d, SI), as already proposed in ref 36. The method assumes that the melting enthalpy of a 100% crystalline sample is 42 ± 8 J g^{-1}. DSC methods are instead unavailable for sPS, due to the occurrence of many phase transitions before melting.

The optical transmittance of polymer films, with thicknesses in the range of 50−60 μm, was measured by using a Shimadzu UV−visible spectrophotometer (UV-2600). Films, after guest removal, were placed between two quartz plates, and the transmittance was measured as a function of wavelength in the 200−800 nm range.

Scanning electron microscopy (Carl Zeiss SMT AG, Oberkochen, Germany) was used to study the surface morphology of polymer films. Before imaging, all of the films were coated with a thin layer of gold to protect the sample from beam damage (Agar auto sputter coater model 108 A, Stansted, UK).

RESULTS AND DISCUSSION

sPS and PPO Films with Different Planar Orientations of Their NC Phases. The kind and degree of the planar orientation of crystalline phases of polymer films can be determined by sending the X-ray beam parallel to the film plane and by collecting 2D-WAXD patterns with the so-called EDGE geometry.[28−34] 2D-WAXD EDGE patterns of NC films of sPS (a,b) and PPO (c,d), as obtained from the corresponding CC films after guest extraction, are shown in Figure 1. sPS films

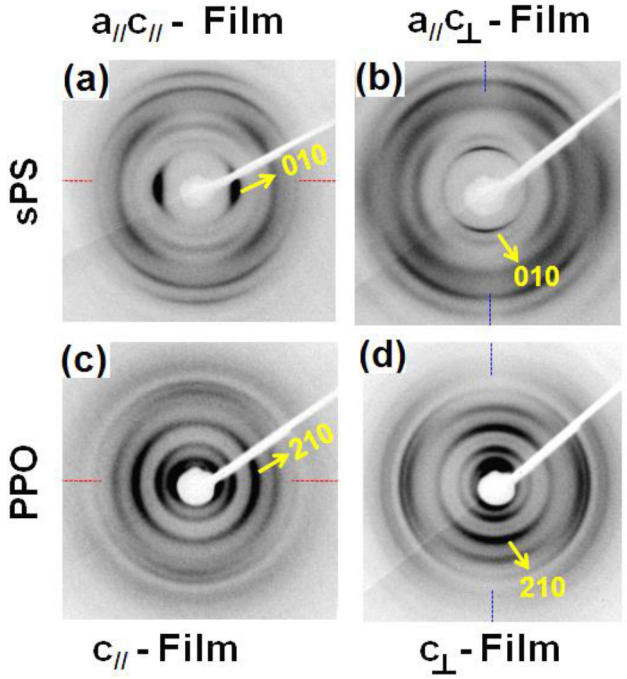

Figure 1. 2D-WAXD EDGE patterns for NC sPS (a, b) and NC PPO (c, d) films, as obtained by guest extraction from CC films. NC sPS films: (a) cast from $CHCl_3$ solution, $a_{\parallel}c_{\parallel}$ orientation; (b) cast from p-xylene solution, $a_{\parallel}c_{\perp}$ orientation. NC PPO films: (c) cast from BE solution, $c_{\parallel}$ orientation; (d) crystallized by immersion of an amorphous film in BE, $c_{\perp}$ orientation. Miller indexes of relevant reflections of the δ-form of sPS and of the α-form of PPO are indicated close to observed diffraction arcs.

measured in parts a and b of Figure 1 were obtained by casting from $CHCl_3$ and p-xylene solutions, respectively. PPO films used for parts c and d of Figure 1 were obtained by dibenzyl ether (BE) solution casting and by immersion of an amorphous film in BE, respectively.

Patterns of Figure 1a,c show centered on the equator (red dotted line) diffraction arcs corresponding to $hk0$ reflections, for instance, 010 and 210, of the NC δ-form of sPS and of the NC α-form of PPO, respectively. This indicates the occurrence for both polymers of $c_{\parallel}$ orientation. More in detail for sPS, the

https://doi.org/10.1021/acs.macromol.1c00925
Macromolecules 2021, 54, 6605−6611

pattern of Figure 1a shows the centering on the equator of only the 0k0 (010 and 020) reflections, thus indicating the occurrence of the uniplanar $a_{\parallel}c_{\parallel}$ crystalline phase orientation.[29,30] Patterns of Figure 1b,d show as centered on the meridian (blue dotted line) diffraction arcs corresponding to hk0 reflections of the NC δ-form of sPS and of the NC α-form of PPO, respectively. This indicates the occurrence for both polymers of $c_{\perp}$ orientation.[32] More in detail for sPS, the pattern of Figure 1b indicates the occurrence of the uniplanar $a_{\parallel}c_{\perp}$ crystalline phase orientation.[29,30]

Simplified presentations of the observed $c_{\parallel}$ and $c_{\perp}$ planar orientations of the crystalline phases are shown in parts a and b of Figure 2, respectively. These orientations could correspond to crystalline lamellae being edge-on and flat-on the film surface, respectively.

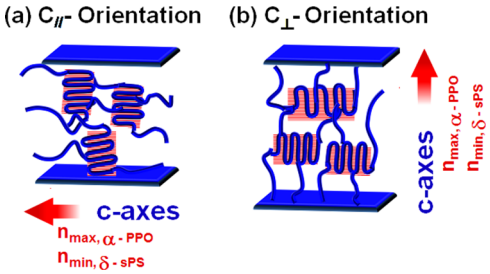

Figure 2. Simplified presentation of planar orientations of the NC phases observed for sPS and PPO: (a) $c_{\parallel}$ orientation, possibly corresponding to crystalline lamellae being edge-on to the film surface, and (b) $c_{\perp}$ orientation, possibly corresponding to crystalline lamellae being flat-on to the film surface. The directions of the chain axes correspond to minimum and maximum values of the refractive index of the NC δ-form of sPS and of the NC α-form of PPO, respectively.

The degree of planar or uniplanar orientation, as evaluated by azimuthal scans as described in the Experimental Section, is negative for the $a_{\parallel}c_{\perp}$-oriented sPS (Figure 1b, $f_c = -0.22$) and for the $c_{\perp}$-oriented PPO (Figure 1d, $f_c = -0.3$) films, while it is positive for the $a_{\parallel}c_{\parallel}$-oriented sPS (Figure 1a, $f_c = +0.71$) and $c_{\parallel}$-oriented PPO (Figure 1c, $f_c = +0.45$) films.

This kind of structural analysis has been conducted for many sPS and PPO films, as obtained by using many different guests as well as different preparation procedures (solution casting or guest-induced crystallization of amorphous films). Crystal phases, kind and degree of planar orientation, and density of the obtained sPS and PPO films are shown in Tables 1 and 2, respectively.

Visual Transparency and UV−Visible Transmittance of sPS and PPO NC Films. The sPS and PPO films, whose preparation procedure and kind and degree of planar orientations are collected in Tables 1 and 2, respectively, have been characterized as for their optical transparency.

As a general trend, sPS films with the $c_{\parallel}$ orientation are more transparent than sPS films with the $c_{\perp}$ orientation, while the opposite is true for PPO films, with the $c_{\parallel}$ orientation being less transparent than the $c_{\perp}$ orientation. This is shown, for instance, by the photographs in Figure 3a−d of sPS and PPO films for which the WAXD patterns are shown in Figure 1a−d, respectively. For the sake of comparison, photographs of the corresponding sPS and PPO amorphous transparent films are shown on the right side of Figure 3.

Quantitative evaluations of the transparency have been conducted with UV−visible spectra, in the range of 200−800 nm, for sPS and PPO films with thicknesses of 50−60 μm (parts a and b of Figure 4, respectively). Of course, the maximum transparency occurs for amorphous films (black lines). The spectra of Figure 4 clearly confirm the opposite behavior of the two NC polymers, which is already suggested by a visual inspection of the films (Figure 3). The transparency of sPS films (Figure 4a) is high for the $c_{\parallel}$ orientation (green curves) and low for the $c_{\perp}$ orientation (red curves), while the transparency of PPO films (Figure 4b), on the contrary, is high for the $c_{\perp}$ orientation (red curves) and low for the $c_{\parallel}$ orientation (green curves). Intermediate transparency occurs for unoriented films of both polymers (blue curves in Figure 4).

The comparison is particularly significant for the sPS films of Figure 4a, because all of the compared semicrystalline films were prepared by room temperature casting of 0.5 wt % polymer solutions and exhibit the same NC form (δ) with similar density [in the range of 0.996−1.006 g/cm^3 (fifth column of Table 1), corresponding to a degree of crystallinity in the range of 34−43%].

As for PPO, particularly interesting is the comparison between spectra of NC films all exhibiting the same NC form (α),[36] as well as a similar degree of crystallinity, as pointed out by similar experimental density values (0.988 ± 0.006 g/cm^3) being much lower than that of the amorphous sample (1.043 g/cm^3). In fact, the three films with $c_{\perp}$ orientation (red curves) exhibit a transparency close to that of the isotropic amorphous film. All the films with the $c_{\parallel}$ orientation (green curves), independently of the crystallization procedure as well as of the chemical nature of the crystallizing guest, exhibit much lower transmittance values (Figure 4b).

A simple way to compare the transparencies of the prepared sPS and PPO films is the evaluation of the film transmittance at a fixed wavelength in the visible range. Transmittance values at

Table 1. Crystal Phase (δ), Kind of Orientation, Degree of Orientation, Preparation Procedures, Guest Used for Preparation of the Corresponding Cocrystalline Films, Degree of Crystallinity (FTIR), and Transmittance at 600 nm of NC sPS Films (~50−60 μm)

crystal phase, orientation	degree of orientation f_c(010) (±0.05)	preparation procedure	guest	degree of crystallinity (%)	transmittance at 600 nm (%)
amorphous	-	melt quenching	-	-	92
δ, $c_{\perp}$	−0.28	solution cast at rt	TCE	39	38
δ, $c_{\perp}$	−0.3	solution cast at rt	DCE	34	45
δ, $c_{\perp}$	−0.22	solution cast at rt	*p*-xylene	40	35
δ, unoriented	0	solution cast at rt	THF	35	70
δ, $c_{\parallel}$	+0.71	solution cast at rt	$CHCl_3$	43	82
δ, $c_{\parallel}$	+0.8	solution cast at rt	benzene	38	86

https://doi.org/10.1021/acs.macromol.1c00925
Macromolecules 2021, 54, 6605−6611

Table 2. Crystal Phase (α or β), Kind of Orientation, Degree of Orientation, Preparation Procedures, Guest Used for Preparation of the Corresponding Cocrystalline Films, Degree of Crystallinity (DSC), and Transmittance at 600 nm of NC PPO Films (~50−60 μm)

crystal phase and orientation	degree of orientation $f_c(001)$ (±0.05)	preparation procedure	guest	degree of crystallinity (%)	transmittance at 600 nm (%)
amorphous	-	solution cast at 60 °C	$CHCl_3$	-	90
α, $c_\perp$	−0.3	immersion of amorphous film in liquid guest at rt	BE	44	83
α, $c_\perp$	−0.2	immersion of amorphous film in liquid guest at rt	carvone	41	81
α, $c_\perp$	−0.21	immersion of amorphous film in liquid guest at rt	limonene	37	84
α, $c_\parallel$	+0.4	immersion of amorphous film in liquid guest at rt	TCA	51	40
α, $c_\parallel$	+0.45	immersion of amorphous film in liquid guest at rt	TCB	53	38
α, $c_\parallel$	+0.45	solution cast at rt or 60 °C	BE, 60 °C	43	33
α, $c_\parallel$	+0.4	solution cast at rt or 60 °C	carvone, 60 °C	49	37
α, $c_\parallel$	+0.45	solution cast at rt or 60 °C	limonene, 60 °C	44	39
α, $c_\parallel$	+0.4	solution cast at rt or 60 °C	TCB, rt	58	47
α, $c_\parallel$	+0.45	solution cast at rt or 60 °C	TCA, rt	51	34
β, unoriented	0	solution cast at rt or 60 °C	$CHCl_3$, rt	41	73
β, unoriented	0	solution cast at rt or 60 °C	DCE, rt	39	69

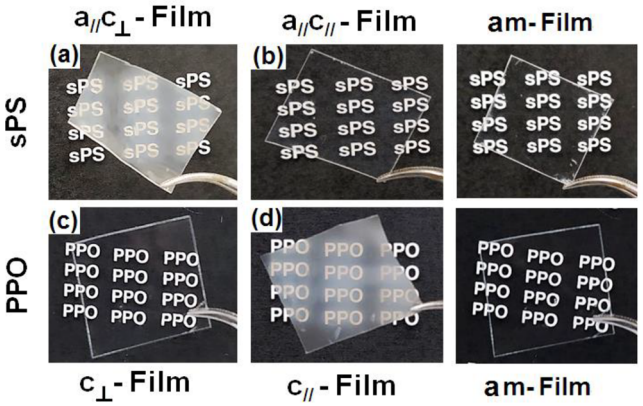

Figure 3. Photographs of sPS and PPO films with a thickness of nearly 60 μm: sPS NC films exhibiting (a) the $a_\parallel c_\perp$ orientation and (b) the $a_\parallel c_\parallel$ orientation and PPO NC films exhibiting (c) the $c_\perp$ orientation and (d) the $c_\parallel$ orientation. On the right side of the figure are photographs of fully amorphous (am) sPS and PPO films.

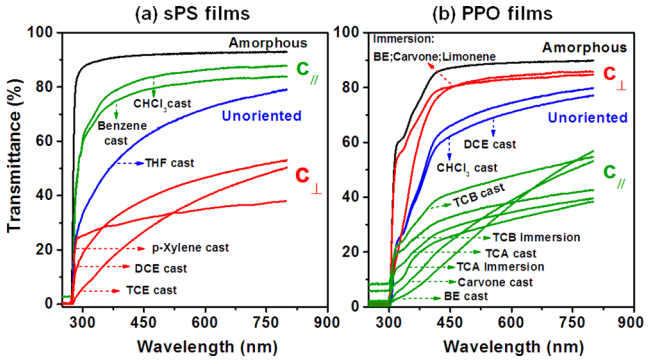

Figure 4. UV−visible spectra of sPS (a) and PPO (b) films having thicknesses in the 50−60 μm range: (black line) amorphous, (red lines) NC films with the $c_\perp$ orientation, (blue lines) unoriented NC films, and (green lines) NC films with the $c_\parallel$ orientation. Guests of the starting CC films and crystallization procedures used, i.e., solution casting (cast) or induced by immersion in the liquid guest (immersion), are indicated close to the curves.

600 nm of all the prepared films are collected in the last columns of Tables 1 and 2.

It is worth adding that SEM images of sPS and PPO films are poorly dependent on the kind of crystalline phase planar orientation. For instance, SEM images for films for which the WAXD patterns are shown in Figure 1a−d are shown in Figure S1a−d, respectively. Both SEM images of sPS with $a_\parallel c_\parallel$ (Figure S3a) and $a_\parallel c_\perp$ (Figure S3b) orientations show very small microstructures and smooth surfaces. Both SEM images of PPO with $c_\parallel$ (Figure S3c) and $c_\perp$ (Figure S3d) orientations show slightly larger microstructures and rough surfaces. Moreover, also correlation lengths of polymer crystallites, as evaluated by the full width at half-maximum (fwhm) of the crystalline reflections of the patterns of Figure 1, do not change significantly with the kind of planar orientation. For instance, the correlation length (as evaluated by the method described in the Experimental Section) for the 301/$\bar{3}$21 reflection of the δ-form of sPS is similar for films with $a_\parallel c_\parallel$ and $a_\parallel c_\perp$ orientations of Figure 1a,b (7.6 ± 0.1 nm). Analogously, correlation length for the 210 reflection of the α-form of PPO is similar for films with $c_\parallel$ and $c_\perp$ of Figure 1c,d (4.8 and 5.4 nm, respectively, i.e., even higher for the more transparent film with $c_\perp$ orientation). Hence, microscopic images and WAXD patterns indicate that the observed dependence of transparency on the crystalline phase orientation is not due to different sizes of polymer crystallites.

All of the above-reported data refer to sPS and PPO films exhibiting a thickness in the range of 50−60 μm. Similar results are obtained for different film thicknesses, at least for the range of 20−100 μm, as shown by the UV−visible spectra of Figure 5.

Interpretation of the Opposite Effects of Planar Orientations on the Transparency of NC Films. The opposite dependence of film transparency on $c_\parallel$ and $c_\perp$ orientations (as shown by the data of Figures 4 and 5 and of the last columns of Tables 1 and 2) can be rationalized, on the basis of the opposite birefringence of the two polymers.

The negative birefringence for sPS films[37−40] and fibers[41] and positive birefringence for PPO films[42−44] are well-established and easily rationalized by the phenyl rings being nearly perpendicular[7] and parallel[45] to the crystalline polymer chain axes, respectively. For instance, the intrinsic birefringences of PS and PPO, as evaluated in ref 42, are −0.10 and +0.21, respectively.

NC phases of both sPS and PPO are less dense than the corresponding amorphous phases ($d_{NC} < d_{am}$), and hence, both

https://doi.org/10.1021/acs.macromol.1c00925
Macromolecules 2021, 54, 6605−6611

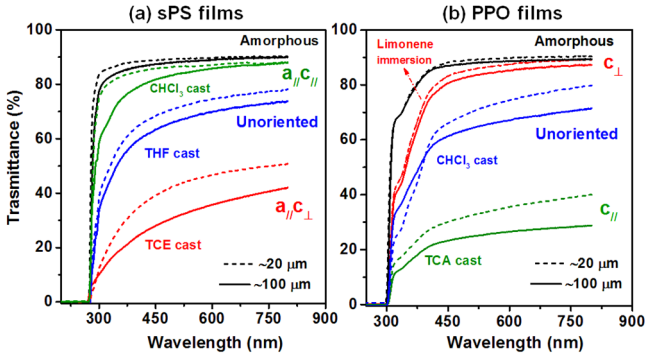

Figure 5. UV−visible spectra of sPS (a) and PPO (b) films having thicknesses of nearly 20 μm (dashed lines) and 100 μm (continuous lines): (black) amorphous, (red) NC films with $c_\perp$ orientation, (blue) unoriented NC films, and (green) NC films with $c_\parallel$ orientation. Guests of the starting CC films and the crystallization procedures used are indicated close to the curves.

exhibit lower values of refractive indexes with respect to the corresponding amorphous phases ($n_{NC} < n_{am}$), as shown by measurements on both sPS films[39] and PPO films.[46]

For instance, the density of amorphous PPO films (1.043 g/cm^3)[45] is definitely higher than for NC α-form PPO films (in the range of 098−0.99 g/cm^3; see Table 1 in ref 45) and the extrapolation of these data to 100% crystallinity gives a density of the NC α-form of nearly 0.93 g/cm^3. Correspondingly, the refractive index of the α-form NC PPO film is lower by 3−6% with respect to the refractive index of amorphous PPO films (1.56 at 1000 nm; see Figure 2 in ref 46). This indicates that the refractive index of the NC α-form is lower by roughly 10% with respect to the refractive index of the corresponding amorphous phase.

To maximize the transparency of any semicrystalline polymer film it is relevant to have orientations of the refractive index ellipsoid (associated with the crystalline phase) with its component perpendicular to the film plane being nearly equal to the refractive index of the amorphous phase. This condition for NC phases can be approached by orienting crystallites with long axes of their refractive index ellipsoid (n_0 for negative birefringence and n_c for positive birefringence) being perpendicular to the film plane (Figure 6). Hence, negatively birefringent sPS NC phases and positively birefringent PPO NC phases maximize their transparency by the $c_\parallel$ orientation (Figure 6a) and the $c_\perp$ orientation (Figure 6b), respectively.

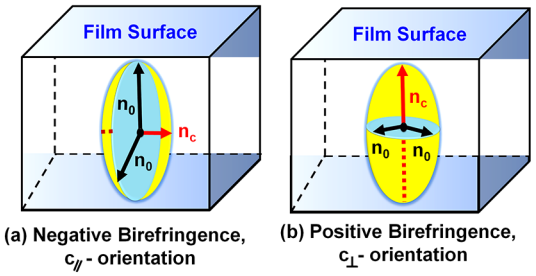

Figure 6. Schematic presentation of crystalline-phase planar orientations that maximize transparency of NC films: (a) $c_\parallel$ orientation, for negatively birefringent sPS films ($n_c < n_0$), and (b) $c_\perp$ orientation, for positively birefringent PPO films ($n_c > n_0$). The high transparency would be due to the orientation of the refractive index ellipsoids with a long axis (n_0 in a and n_c in b) perpendicular to the film plane.

In summary, the transparency of the prepared NC films is dominated by their crystal phase orientation. In particular, maximum transparency values are obtained when a long axis of the refractive index ellipsoid (associated with the NC structure) is perpendicular to the film plane. This corresponds to the $c_\parallel$ orientation for the negatively birefringent sPS and the $c_\perp$ orientation for the positively birefringent PPO.

CONCLUSION

Crystalline phase orientation in polymer films can have a strong influence on film transparency, because crystalline phases are generally optically anisotropic.

Quantitative evaluations of the transparency of sPS and PPO films, conducted with UV−visible spectra, show an opposite behavior of the two NC polymers: transparency of sPS films is favored by the $c_\parallel$ orientation, while transparency of PPO films, on the contrary, is favored by the $c_\perp$ orientation.

The observed behavior can be rationalized by considering negative and positive birefringence (i.e., lower and higher refractive index parallel to the crystalline chain axis) of sPS and PPO crystalline phases, respectively. In fact, the $c_\parallel$ orientation for sPS and the $c_\perp$ orientation for PPO lead long axes of their refractive index ellipsoids to be preferentially perpendicular to the film plane (Figure 6). In this way, the refractive index of the NC phase, in the direction perpendicular to the film plane, becomes closer to the refractive index of the denser amorphous phase.

The increase of transparency is of course relevant for all polymers. Transparency is, however, particularly relevant for NC films (mainly for their applications in optical sensors)[46,47] as well as for CC films including dye,[48] fluorescent,[49] and photoreactive[50,51] guest molecules.

ASSOCIATED CONTENT

Supporting Information

The Supporting Information is available free of charge at https://pubs.acs.org/doi/10.1021/acs.macromol.1c00925.

WAXD radial profiles (Figure S1), correlation length (D) values (Table S1), FTIR and DSC patterns (Figure S2), and SEM images (Figure S3) (PDF)

AUTHOR INFORMATION

Corresponding Author

Gaetano Guerra − *Dipartimento di Chimica e Biologia, INSTM Research Unit, Università di Salerno, 84084 Fisciano, SA, Italy;* orcid.org/0000-0003-1576-9384; Email: gguerra@unisa.it

Authors

Baku Nagendra − *Dipartimento di Chimica e Biologia, INSTM Research Unit, Università di Salerno, 84084 Fisciano, SA, Italy*

Paola Rizzo − *Dipartimento di Chimica e Biologia, INSTM Research Unit, Università di Salerno, 84084 Fisciano, SA, Italy;* orcid.org/0000-0002-3375-3119

Christophe Daniel − *Dipartimento di Chimica e Biologia, INSTM Research Unit, Università di Salerno, 84084 Fisciano, SA, Italy*

Complete contact information is available at: https://pubs.acs.org/10.1021/acs.macromol.1c00925

Author Contributions

All authors contributed equally to this manuscript and approved the final version.

Notes

The authors declare no competing financial interest.

■ ACKNOWLEDGMENTS

Financial support of "Ministero dell'Università e della Ricerca" is gratefully acknowledged. The authors thank Dr. Ivano Immediata for useful discussions.

■ REFERENCES

(1) Macauley, N. J.; Harkin-Jones, E. M. A.; Murphy, W. R. The influence of nucleating agents on the extrusion and thermoforming of polypropylene. *Polym. Eng. Sci.* **1998**, *38*, 516−523.
(2) Gahleitner, M.; Jääskeläinen, P.; Ratajski, E.; Paulik, C.; Reussner, J.; Wolfschwenger, J.; Neißl, W. Propylene−ethylene random copolymers: Comonomer effects on crystallinity and application properties. *J. Appl. Polym. Sci.* **2005**, *95*, 1073−1081.
(3) Daniel, C.; Avallone, A.; Guerra, G. Syndiotactic Polystyrene Physical Gels: Guest Influence on Structural Order in Molecular Complex Domains and Gel Transparency. *Macromolecules* **2006**, *39*, 7578−7582.
(4) Bernland, K.; Tervoort, T.; Smith, P. Phase behavior and optical and mechanical properties of the binary system isotactic polypropylene and the nucleating/clarifying agent 1,2,3-trideoxy-4,6:5,7-bis-*O*-[(4-propylphenyl) methylene]-nonitol. *Polymer* **2009**, *50*, 2460−2464.
(5) Gahleitner, M.; Grein, C.; Blell, R.; Wolfschwenger, J.; Koch, T.; Ingolic, E. Sterilization of propylene/ethylene random copolymers: Annealing effects on crystalline structure and transparency as influenced by polymer structure and nucleation. *eXPRESS Polym. Lett.* **2011**, *5*, 788−798.
(6) Kusanagi, H.; Takase, M.; Chatani, Y.; Tadokoro, H. Crystal structure of isotactic poly(4-methyl-1-pentene. *J. Polym. Sci., Polym. Phys. Ed.* **1978**, *16*, 131−142.
(7) De Rosa, C.; Guerra, G.; Petraccone, V.; Pirozzi, B. Crystal structure of the emptied clathrate form (δe form) of syndiotactic polystyrene. *Macromolecules* **1997**, *30*, 4147−4152.
(8) Petraccone, V.; Ruiz de Ballesteros, O.; Tarallo, O.; Rizzo, P.; Guerra, G. Nanoporous polymer crystals with cavities and channels. *Chem. Mater.* **2008**, *20*, 3663−3668.
(9) Acocella, M. R.; Rizzo, P.; Daniel, C.; Tarallo, O.; Guerra, G. Nanoporous triclinic δ modification of syndiotactic polystyrene. *Polymer* **2015**, *63*, 230−236.
(10) Daniel, C.; Longo, S.; Vitillo, J. G.; Fasano, G.; Guerra, G. Nanoporous Crystalline Phases of Poly(2,6-dimethyl-1,4-phenylene)-oxide. *Chem. Mater.* **2011**, *23*, 3195−3200.
(11) Daniel, C.; Pellegrino, M.; Venditto, V.; Aurucci, S.; Guerra, G. Nanoporous-crystalline poly(2,6-dimethyl-1,4-phenylene)oxide (PPO) aerogels. *Polymer* **2016**, *105*, 96−103.
(12) Corradini, P.; Petraccone, V.; De Rosa, C.; Guerra, G. On the structure of the quenched mesomorphic phase of isotactic poly-propylene. *Macromolecules* **1986**, *19*, 2699−2703.
(13) Cavallo, D.; Portale, G.; Balzano, L.; Azzurri, F.; Bras, W.; Peters, G. W.; Alfonso, G. C. Real-Time WAXD Detection of Mesophase Development during Quenching of Propene/Ethylene Copolymers. *Macromolecules* **2010**, *43*, 10208−10212.
(14) Stein, R. S. Optical studies of the stress-induced crystallization of polymers. *Polym. Eng. Sci.* **1976**, *16*, 152−157.
(15) Mahendrasingam, A.; Martin, C.; Fuller, W.; Blundell, D. J.; Oldman, R. J.; MacKerron, D. H.; Harvie, J. L.; Riekel, C. Observation of a transient structure prior to strain-induced crystallization in poly(ethylene terephthalate). *Polymer* **2000**, *41*, 1217−1221.
(16) Gorlier, E.; Haudin, J. M.; Billon, N. Strain-induced crystallisation in bulk amorphous PET under uni-axial loading. *Polymer* **2001**, *42*, 9541−9549.
(17) Somani, R. H.; Yang, L.; Hsiao, B. S.; Sun, T.; Pogodina, N. V.; Lustiger, A. Shear-Induced Molecular Orientation and Crystallization in Isotactic Polypropylene: Effects of the Deformation Rate and Strain. *Macromolecules* **2005**, *38*, 1244−1255.
(18) Stoclet, G.; Seguela, R.; Lefebvre, J. M.; Elkoun, S.; Vanmansart, C. Strain-Induced Molecular Ordering in Polylactide upon Uniaxial Stretching. *Macromolecules* **2010**, *43*, 1488−1498.
(19) Binsbergen, F. L. Orientation-induced nucleation in polymer crystallization. *Nature* **1966**, *211*, 516−17.
(20) Swartjes, F. H. M.; Peters, G. W. M.; Rastogi, S.; Meijer, H. E. H. Stress induced crystallization in elongational flow. *Int. Polym. Process.* **2003**, *18*, 53−66.
(21) Tsai, C.-C.; Wu, R.-J.; Cheng, H.-Y.; Li, S.-C.; Siao, Y.-Y.; Kong, D.-C.; Jang, G.-W. Crystallinity and dimensional stability of biaxial oriented poly(lactic acid) films. *Polym. Degrad. Stab.* **2010**, *95*, 1292−1298.
(22) Pantani, R.; Coccorullo, I.; Volpe, V.; Titomanlio, G. Shear-Induced Nucleation and Growth in Isotactic Polypropylene. *Macromolecules* **2010**, *43*, 9030−9038.
(23) Ma, Z.; Fernandez-Ballester, L.; Cavallo, D.; Gough, T.; Peters, G. W. M. High-Stress Shear-Induced Crystallization in Isotactic Polypropylene and Propylene/Ethylene Random Copolymers. *Macromolecules* **2013**, *46*, 2671−2680.
(24) Samuels, R. J. Morphology of deformed polypropylene. Quantitative relations by combined x-ray, optical, and sonic methods. *J. Polym. Sci., Part A: Gen. Pap.* **1965**, *3*, 1741−1763.
(25) Hardaker, S. S.; Moghazy, S.; Cha, C. Y.; Samuels, R. J. Quantitative characterization of optical anisotropy in high refractive index films. *J. Polym. Sci., Part B: Polym. Phys.* **1993**, *31*, 1951−1963.
(26) Prattipati, V.; Hu, Y. S.; Bandi, S.; Mehta, S.; Schiraldi, D. A.; Hiltner, A.; Baer, E. Improving the transparency of stretched poly(ethylene terephthalate)/polyamide blends. *J. Appl. Polym. Sci.* **2006**, *99*, 225−235.
(27) Heffelfinger, C. J.; Burton, R. L. X-Ray determination of the crystallite orientation distributions of polyethylene terephthalate films. *J. Polym. Sci.* **1960**, *47*, 289−306.
(28) Rizzo, P.; Lamberti, M.; Albunia, A. R.; Ruiz de Ballesteros, O.; Guerra, G. Crystalline orientation in syndiotactic polystyrene cast films. *Macromolecules* **2002**, *35*, 5854−5860.
(29) Rizzo, P.; Spatola, A.; De Girolamo Del Mauro, A.; Guerra, G. Polymeric films with three different uniplanar crystalline phase orientations. *Macromolecules* **2005**, *38*, 10089−10094.
(30) Albunia, A. R.; Rizzo, P.; Tarallo, O.; Petraccone, V.; Guerra, G. Layers of close-packed alternated enantiomorphous helicies and the three different uniplanar orientations of syndiotactic polystyrene. *Macromolecules* **2008**, *41*, 8632−8642.
(31) Albunia, A. R.; Rizzo, P.; Guerra, G. Polymeric films with three different orientations of crystalline-phase empty channels. *Chem. Mater.* **2009**, *21*, 3370−3375.
(32) Rizzo, P.; Albunia, A. R.; Guerra, G. Two different uniplanar-axial orientations of syndiotactic polystyrene films. *Macromolecules* **2011**, *44*, 5671−5681.
(33) Rizzo, P.; Ianniello, G.; Longo, S.; Guerra, G. Uniplanar Orientations and Guest Exchange in PPO Cocrystalline Films. *Macromolecules* **2013**, *46*, 3995−4001.
(34) Rizzo, P.; Gallo, C.; Vitale, V.; Tarallo, O.; Guerra, G. Nanoporous-crystalline films of PPO with parallel and perpendicular polymer chain orientations. *Polymer* **2019**, *167*, 193−201.
(35) Musto, P.; Mensitieri, G.; Cotugno, S.; Guerra, G.; Venditto, V. Probing by Time Resolved FTIR Spectroscopy Mass Transport Molecular Interactions, and Conformational Ordering in the System Chloroform Syndiotactic Polystyrene. *Macromolecules* **2002**, *35*, 2296−2304.
(36) Bair, H. E.; Kwei, T. K. Anomalous melting of poly(phenylene oxide). *J. Therm. Anal. Calorim.* **2000**, *59*, 541−546.
(37) Hsiung, C. M.; Cakmak, M. Optical properties and orientation development in uniaxially stretched syndiotactic polystyrene from amorphous precursors. On-line deformation behavior. *Int. Polym. Process.* **1992**, *7*, 51−59.

https://doi.org/10.1021/acs.macromol.1c00925
Macromolecules 2021, 54, 6605−6611

(38) Yan, R. J.; Ajji, A.; Shinozaki, D. M.; Dumoulin, M. M. Uniaxial drawing behavior of syndiotactic polystyrene. *Polymer* **2000**, *41*, 1077−1086.
(39) Rizzo, P.; Costabile, A.; Guerra, G. Perpendicular Orientation of Host Polymer Chains in Clathrate Thick Films. *Macromolecules* **2004**, *37*, 3071−3076.
(40) Rizzo, P.; Albunia, A. R.; Guerra, G. Negatively Birefringent Polymer Films. *Macromol. Chem. Phys.* **2009**, *210*, 2148−2152.
(41) Hada, Y.; Shikuma, H.; Ito, H.; Kikutani, T. Structure and properties of syndiotactic polystyrene fibers prepared in high-speed melt spinning process. *Fibers Polym.* **2005**, *6*, 19−27.
(42) Lefebvre, D.; Jasse, B.; Monnerie, L. Evaluation of the birefringence of uniaxially oriented poly(2,6-dimethyl 1,4-phenylene oxide)-atactic polystyrene blends. *Polymer* **1982**, *23*, 706−709.
(43) Machell, J. S.; Greener, J.; Contestable, B. A. Optical properties of solvent-cast polymer films. *Macromolecules* **1990**, *23*, 186−194.
(44) Golla, M.; Nagendra, B.; Rizzo, P.; Daniel, C.; Ruiz de Ballesteros, O.; Guerra, G. Polymorphism of Poly(2,6-dimethyl-1,4-phenylene)oxide in Axially Stretched Films. *Macromolecules* **2020**, *53*, 2287−2294.
(45) Nagendra, B.; Cozzolino, A.; Daniel, C.; Rizzo, P.; Guerra, G.; Auriemma, F.; De Rosa, C.; D'Alterio, M. C.; Tarallo, O.; Nuzzo, A. Two Nanoporous Crystalline Forms of Poly(2,6-dimethyl-1,4-phenylene)oxide and Related Co-Crystalline Forms. *Macromolecules* **2019**, *52*, 9646−9656.
(46) Lova, P.; Bastianini, C.; Giusto, P.; Patrini, M.; Rizzo, P.; Guerra, G.; Iodice, M.; Soci, C.; Comoretto, D. Label-Free Vapor Selectivity in Poly(p-Phenylene Oxide) Photonic Crystal Sensors. *ACS Appl. Mater. Interfaces* **2016**, *8*, 31941−31950.
(47) Pilla, P.; Cusano, A.; Cutolo, A.; Giordano, M.; Mensitieri, G.; Rizzo, P.; Sanguigno, L.; Venditto, V.; Guerra, G. Molecular sensing by nanoporous crystalline polymers. *Sensors* **2009**, *9*, 9816−9857.
(48) Uda, Y.; Kaneko, F.; Tanigaki, N.; Kawaguchi, T. The First Example of a Polymer-Crystal−Organic-Dye Composite Material: The Clathrate Phase of Syndiotactic Polystyrene with Azulene. *Adv. Mater.* **2005**, *17*, 1846−1850.
(49) De Girolamo Del Mauro, A.; Carotenuto, M.; Venditto, V.; Petraccone, V.; Scoponi, M.; Guerra, G. Fluorescence of Syndiotactic Polystyrene/Trimethylbenzene Clathrate and Intercalate Co-Crystals. *Chem. Mater.* **2007**, *19*, 6041−6046.
(50) Stegmaier, P.; De Girolamo Del Mauro, A.; Venditto, V.; Guerra, G. Optical recording materials based on photoisomerization of guest molecules of a polymeric crystalline host phase. *Adv. Mater.* **2005**, *17*, 1166−1168.
(51) Albunia, A. R.; Rizzo, P.; Coppola, M.; De Pascale, M.; Guerra, G. Azobenzene isomerization in polymer co-crystalline phases. *Polymer* **2012**, *53*, 2727−2735.

https://doi.org/10.1021/acs.macromol.1c00925
Macromolecules 2021, 54, 6605−6611